Spin-polarized tunneling spectroscopy of fully epitaxial magnetic tunnel junctions using $Co_2FeAl_{0.5}Si_{0.5}$ Heusler alloy electrodes

Hiroaki Sukegawa,[1,*] Wenhong Wang,[1] Rong Shan,[1] Tomoya Nakatani,[2] Koichiro Inomata,[1] and Kazuhiro Hono[1,2]
[1]*Magnetic Materials Center, National Institute for Materials Science (NIMS), 1-2-1 Sengen, Tsukuba 305-0047, Japan*
[2]*Graduate School of Pure and Applied Sciences, University of Tsukuba, Tsukuba 305-8571, Japan*
(Received 16 June 2008; revised manuscript received 3 March 2009; published 18 May 2009)

Spin-dependent tunneling spectroscopy has been studied in fully epitaxial magnetic tunnel junctions with full-Heusler $Co_2FeAl_{0.5}Si_{0.5}$ (CFAS) alloys. We fabricated CFAS/MgO/CFAS structures with $L2_1$- and $B2$-ordered CFAS layers and measured the bias voltage dependence of differential conductance G. We found for $L2_1$-CFAS/MgO/$L2_1$-CFAS structure symmetrical conductance curves with respect to polarity of the bias voltage for parallel (P) and antiparallel (AP) magnetization configurations and two characteristic crossovers in G between P and AP accompanied with a flat feature within ± 0.6 V in G (P). On the other hand, only one crossover was observed at a negative-bias voltage for $L2_1$-CFAS/MgO/$B2$-CFAS structure. The direct tunneling that reflects the specific spin-dependent density of states of the half-metallic $L2_1$-CFAS is proposed as a possible transport mechanism leading to the notable crossovers.

DOI: 10.1103/PhysRevB.79.184418 PACS number(s): 75.47.−m, 85.75.−d, 73.20.At, 75.50.Cc

I. INTRODUCTION

Half-metallic compounds which are fully spin polarized near the Fermi level (E_F) due to an energy gap in the minority-spin band[1] have attracted great attention as key materials for creating spintronics devices such as future ultra-high density nonvolatile memory devices and spin metal-oxide-semiconductor field-effect transistor.[2] Especially, Co-based full-Heusler alloys have been intensively studied since the half metallicity is expected even at room temperature (RT) due to their high Curie temperature around 1000 K.[3–16] Recently, a very large tunnel magnetoresistance (TMR) ratio of 570% was achieved in Co_2MnSi(CMS)/AlO_x/CMS magnetic tunneling junctions (MTJs) at 2 K.[11] However, the TMR ratio, which is represented as $2P^2/(1-P^2)$,[17] where P is a tunneling spin polarization, significantly decreases with increasing temperature and becomes 67% at RT. This behavior was attributed to a low-energy separation between Fermi level and conduction-band edge,[11] an inelastic tunneling process including spin flip due to magnon-assisted tunneling[7] through the formation of interface states near E_F in the minority-spin gap[18] or the formation of nonquasiparticle states above E_F in the minority-spin gap,[19] resulting in the low TMR ratio at RT. Recently, we have reported a large TMR ratio at RT and a relatively small temperature dependence of TMR ratio (220% at RT and 390% at 5 K) in epitaxial $Co_2FeAl_{0.5}Si_{0.5}$ (CFAS)/MgO/CFAS MTJs.[14] The TMR ratio of 390% corresponds to $P=0.81$ for CFAS. *Ab initio* calculations on quarternary $Co_2FeAl_{1-x}Si_x$ alloys which were performed after this observation demonstrated the half metallicity of these alloys with the $L2_1$ structure and predicted E_F to be adjustable by controlling the composition x.[20–22] For $x=0.5$ (CFAS) the E_F lies at the middle of the minority-spin gap of about 1 eV, which will enhance the temperature robustness of TMR ratio. This is consistent with the large TMR ratio at RT obtained in the experiment.[14] The low density of states (DOS) of the majority-spin band near E_F in CFAS may also contribute to the relatively small temperature dependence of TMR ratio due to the decreasing of the magnon excitation.

In this paper we report two crossovers in differential tunneling conductance $G=dI/dV$ measured in epitaxial $L2_1$-CFAS/MgO/$L2_1$-CFAS MTJs to discuss the origin of the large TMR ratios obtained in the MTJs. The direct tunneling that reflects the specific spin-dependent DOS of the half-metallic CFAS obtained from the first-principle calculations[20–22] is proposed as a possible transport mechanism leading to the notable crossovers.

II. EXPERIMENTAL DETAILS

Multilayers were deposited on single-crystal MgO (001) substrates using an ultrahigh vacuum magnetron sputtering system with the base pressure below 8×10^{-8} Pa. We used MgO buffer layer in place of Cr buffer layer used in Ref. 14 because Cr buffer impedes a highly $L2_1$-ordered CFAS structure due to the Cr atoms interdiffusion by postannealing at higher temperatures above 723 K and thus limits to achieve higher spin polarization. Typical MTJ structure fabricated is a top-spin-valve type consisting of MgO (20)/CFAS (30)/Mg (0.3)/MgO(1.1 or 1.4)/CFAS (5)/$Co_{75}Fe_{25}$ (2)/$Ir_{20}Mn_{80}$ (15)/Ru (7) (thickness in nm) on MgO (001) substrates. MgO layers were sputter deposited from a sintered MgO target directly using rf magnetron, whereas other metallic layers were deposited using dc magnetron. We inserted the thin Mg layer under the MgO barrier layer in order to avoid the oxidation of the bottom-CFAS layer. CFAS layers were deposited at RT from a stoichiometric target (Co 50.0%, Fe 25.0%, Al 12.5%, and Si 12.5%). After the deposition of the bottom-CFAS layer we postannealed for 15 min *in situ* at $T_{bottom}=813$ K. Postannealing was also performed at T_{top}=RT or 813 K after the deposition of the top-CFAS layer. Finally we annealed the multilayers at 633 K in a furnace under a magnetic field of 5 kOe for 1 h in order to exchange bias the top electrode. Both MTJs (junction area: $5\times2-10\times10$ μm^2) and electrodes were patterned using a typical microfabrication technique, i.e., electron-beam lithography, photolithography, and Ar ion-beam etching. The crystal structure of CFAS films was investigated by x-ray diffraction (XRD).

 ©2009 The American Physical Society

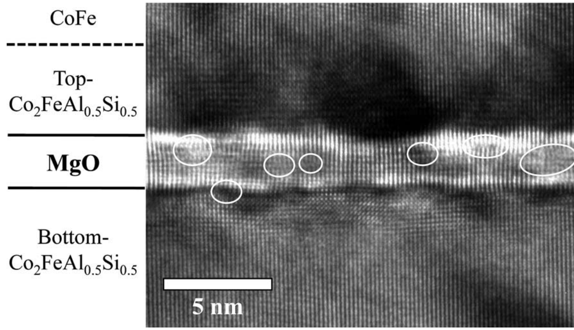

FIG. 1. Cross-sectional high-resolution transmission electron microscopy image of a $L2_1$-CFAS/MgO/$L2_1$-CFAS magnetic tunnel junction along the [110] direction of the CFAS layers. Structural imperfections are circled.

MTJs were characterized by measuring *R-H* (TMR) and current-voltage (*I-V*) curves with a dc four-probe method in a temperature range of 7–290 K, where a magnetic field was applied along CFAS [110] (‖MgO[100]). In this study, the positive current is defined as that electrons flow from the top-CFAS layer to the bottom-CFAS layer. The composition of deposited CFAS films was confirmed to be nearly stoichiometric (Co 51.0%, Fe 23.2%, Al 14.1%, and Si 11.7%) by inductively coupled plasma analysis.

III. RESULTS

A. Structural characterization

Cross-sectional high-resolution transmission electron microscopy (HRTEM) was used to clarify the detailed crystal structure of the multilayer [CFAS(T_a=873 K)/MgO/CFAS(T_a=813 K)]. In the HRTEM lattice image, as shown in Fig. 1, very smooth and abrupt interfaces are realized in the CFAS/MgO/CFAS structure. Both bottom- and top-CFAS layers are grown epitaxially and single crystalline. The lattice spacing of the CFAS layers are resolved with d =0.20 nm, corresponding to body-centered cubic {110} planes. The MgO layer shows a [001] growth orientation, nevertheless a large number of structural imperfections are observed. Interestingly, the defects are introduced not only at the CFAS/MgO interfaces but also inside the MgO layer, which is shown by circles in an MgO barrier to relax the lattice mismatch between MgO and CFAS (approximately 4.7%). In the reports of the epitaxial MTJs with MgO layers prepared using an electron-beam evaporation [Fe/MgO/Fe (Ref. 23) and CMS/MgO/CoFe (Refs. 12 and 16)], in which TMR enhancement due to the coherent tunneling has been observed, almost all lattice dislocations form at the interfaces and the desired epitaxial (001) growth for MgO layer is successfully achieved, unlike in our MgO barrier. Therefore, the coherent tunneling effect would be weakened in our MTJs as well as in the MTJ with the polycrystalline MgO barrier.[24]

B. TMR properties

We prepared MTJs with different ordering of CFAS films by changing the postannealing temperature, in which

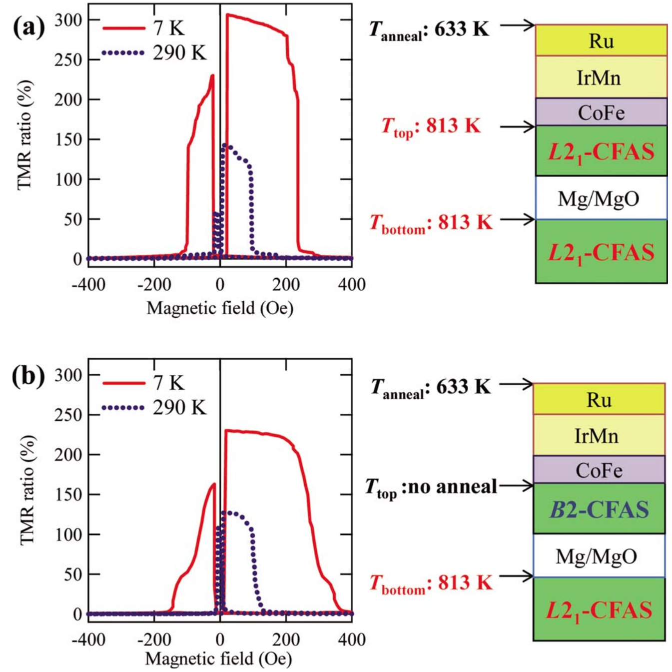

FIG. 2. (Color online) TMR curves and schematic illustrations of magnetic tunnel junctions with (a) $L2_1$-CFAS/MgO(1.1 nm)/$L2_1$-CFAS and (b) $L2_1$-CFAS/MgO(1.4 nm)/$B2$-CFAS structures. Bias voltages of 1 mV (7 K) and 5 mV (RT) were applied for the measurement.

$L2_1$-CFAS/MgO/$L2_1$-CFAS structure was achieved by post-annealing at 813 K for both bottom- and top-CFAS layers (T_{bottom}=813 K and T_{top}=813 K), accompanied with almost perfect (001) orientation and very flat surface with an average surface roughness of 0.10 nm.[25] The $L2_1$-CFAS/MgO/$B2$-CFAS structure was formed when annealed at 813 K for only the bottom-CFAS layer (T_{bottom}=813 K and T_{top} =RT). Thus, we can investigate the $L2_1$ and $B2$ ordering dependences on spin-dependent tunneling properties through the two different structures for the top-CFAS layer.[25] TMR curves at both 7 and 290 K (RT) are shown for a $L2_1$/MgO(1.1 nm)/$L2_1$ structure in Fig. 2(a) and a $L2_1$/MgO(1.4 nm)/$B2$ structure in Fig. 2(b). Bias voltages of 1 mV (7 K) and 5 mV (RT) were applied for the measurement. TMR ratios at RT for both structures are approximately equal, 130–140 %. However a large difference was observed at 7 K, 308% and 227% for the $L2_1$-CFAS/MgO/$L2_1$-CFAS and $L2_1$-CFAS/MgO/$B2$-CFAS structures, respectively, which implies higher P in $L2_1$ than $B2$ at 7 K [$P(L2_1)$=0.78 and $P(B2)$=0.68 determined by Julliere's formula].[17]

The lower tunneling spin polarization of 0.78 than that expected from the half metallicity of the $L2_1$-CFAS suggests that the TMR enhancement due to the coherent tunneling may be negligibly small and the inelastic tunneling process still contributes in our MTJs due to the low-quality MgO barrier as seen in Fig. 1. In fact, TMR ratios of $L2_1$-CFAS/MgO(1.4 nm)/CoFe MTJs on MgO-buffered MgO (001) substrates, which were fabricated using the same process as described in this study and have a degraded MgO barrier as demonstrated in *in situ* reflective high-energy elec-

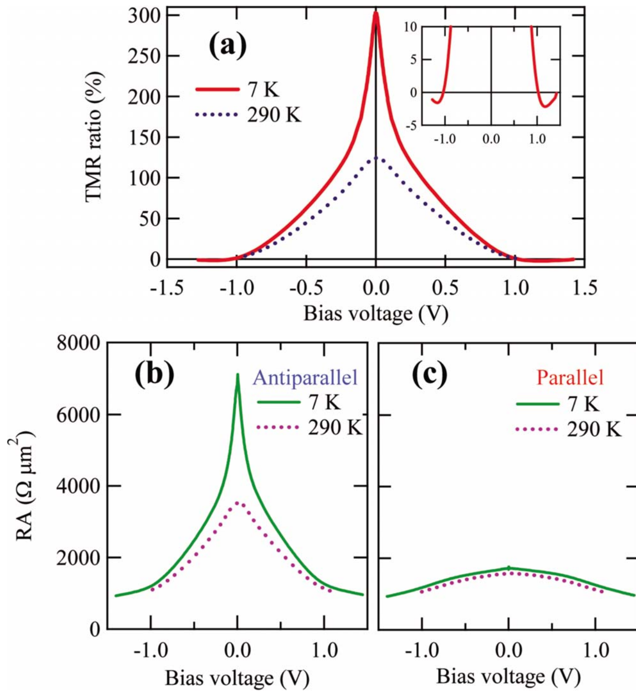

FIG. 3. (Color online) Bias voltage dependences of (a) TMR ratio, (b) resistance area (RA) product of antiparallel state, and (c) RA of parallel state for $L2_1$-CFAS/MgO(1.1 nm)/$L2_1$-CFAS structure. Inset in (a) indicates closeup near 1 V for the TMR curve measured at 7 K.

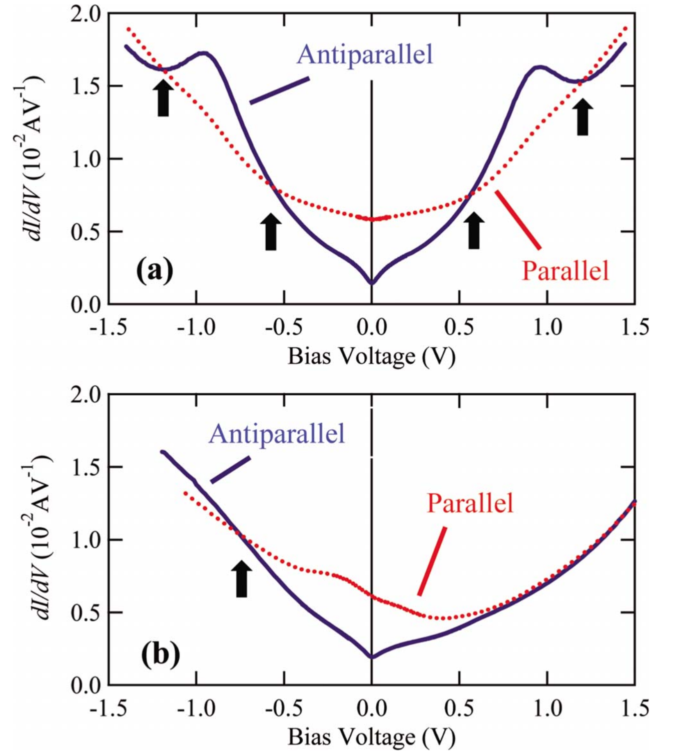

FIG. 4. (Color online) dI/dV spectra of MTJs with (a) $L2_1$-CFAS/MgO(1.1 nm)/$L2_1$-CFAS and (b) $L2_1$-CFAS/MgO(1.4 nm)/$B2$-CFAS structures at 7 K. The dotted lines (solid lines) represent the parallel (antiparallel) magnetization configuration. The arrows represent the points where the parallel and the antiparallel lines cross each other.

tron diffraction, showed TMR of 130% and 95% at 7 K and RT, respectively.[26] These TMR values correspond to tunneling spin polarizations $P_{\mathrm{CoFe}}=0.505$ (7 K) and 0.495 (RT) for CoFe if we assume $P(L2_1\text{-CFAS})=0.78$ and 0.65 (RT) as estimated above. $P_{\mathrm{CoFe}}=0.505$ is close to the value of 0.506 derived from CoFe/AlO_x/CoFe tunnel structures,[27] which also suggests negligibly small TMR enhancement by MgO(001) structure in our MTJs.

Figure 3(a) shows the bias voltage dependences of TMR ratio at 7 and 290 K (RT) and Figs. 3(b) and 3(c) show the resistance for antiparallel (AP) and parallel (P) states as a function of bias voltage at 7 K and RT, respectively. The TMR ratio at 7 K decreases rapidly at a low-bias voltage and gradually in a higher voltage region; however, such sharp-bias voltage dependence of TMR ratios does not appear at RT. Note that the TMR becomes negative over 1 eV as shown in the inset in Fig. 3(a). The resistance change in the low-bias voltage region at 7 K is small for P but is remarkable for AP similar to the TMR change, indicating that the TMR reduction by the bias voltage is originated from the resistance reduction in the AP state.

C. Spin-polarized tunneling spectroscopy

We obtained the bias voltage dependences of dI/dV by the numerical calculation of I-V curves in order to investigate the DOS of the CFAS films. Figure 4(a) shows the result at 7 K for the $L2_1$-CFAS/MgO/$L2_1$-CFAS structure. Symmetrical curves are observed with respect to polarity of the bias voltage for both P (dotted curve) and AP (solid curve) states, indicating similar interface structures for both bottom CFAS/MgO and MgO/top CFAS. A clear dip appears around zero-bias voltage for G_{AP} curve, which is characteristic of the magnon excitation contribution to spin-dependent tunneling as commonly observed in typical MTJs.[28] However, this dip disappears at RT (data not shown). The G_{P} curve of $L2_1$-CFAS/MgO/$L2_1$-CFAS exhibits a small change within ± 0.6 V range as seen in Fig. 4(a). Such a feature has already been reported in the MTJs with half-metallic CMS layers.[11] Additionally, these curves demonstrate a distinguishing feature; two obvious crossovers between G_{P} and G_{AP} at $+(-)0.6$ and $+(-)1.2$ V and a distinct peak in G_{AP} at $+(-)0.9$ V. The two crossovers and the peak in G_{AP} were observed even at RT (data not shown). On the other hand, as shown in Fig. 4(b), the conductance characteristics of the $L2_1$-CFAS/MgO/$B2$-CFAS structure differ considerably from those of the $L2_1$-CFAS/MgO/$L2_1$-CFAS structure, which exhibits the pronounced asymmetry regarding the polarity and a crossover between G_{P} and G_{AP} in the negative-bias voltage region only (electrons flow: $L2_1$-CFAS $\rightarrow B2$-CFAS).

IV. DISCUSSION

We propose the direct tunneling that reflects the specific spin-dependent DOS of the half-metallic bulk CFAS as a possible transport mechanism leading to the notable cross-

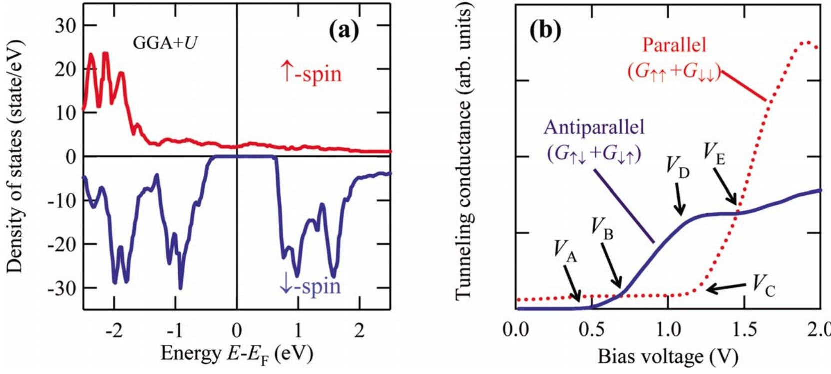

FIG. 5. (Color online) (a) Spin-resolved DOS of $L2_1$-$Co_2FeAl_{0.5}Si_{0.5}$ obtained from the generalized gradient approximation (GGA)+U theorem. (b) Calculated dI/dV spectra based on Fig. 5(a) and Eq. (2) for parallel (dotted line) and antiparallel (solid line) configurations.

overs. In order to clarify the direct tunneling effect, we modeled the calculated bulk band structure of CFAS (Ref. 22) and estimated the tunneling conductance. For simplicity, we assume that the conductance is determined only by DOS of both electrodes and neglect parameters for the tunnel barrier and the possible spin-filtering effect of MgO. Additionally, we assumed no spin-flip process during tunneling for simplicity. This assumption, however, does not change the essential interpretation of the tunneling spectra. If spins of the both electrodes are denoted by σ $(=\uparrow,\downarrow)$ and σ' $(=\uparrow,\downarrow)$, respectively, these assumptions provide tunneling current $I_{\sigma,\sigma'}$ due to σ to σ' spin channel under the application of finite bias voltage V as written in Eq. (1) (Ref. 29):

$$I_{\sigma,\sigma'}(V) = \frac{2\pi e}{\hbar}\int \langle|\hat{T}|^2\rangle D_\sigma(E)D_{\sigma'}(E+eV)[f_\sigma(E) - f_{\sigma'}(E+eV)]dE, \tag{1}$$

where $\langle|\hat{T}|^2\rangle$ represents an averaged tunneling probability and f is the Fermi distribution function. D_σ and $D_{\sigma'}$ represent DOSs for σ and σ' spin bands of both electrodes, respectively. If we consider at $T=0$ K and assume that $\langle|\hat{T}|^2\rangle$ is independent of spin, Eq. (1) is simplified as

$$I_{\sigma,\sigma'}(V) = G_{\sigma,\sigma'}V = \frac{2\pi e}{\hbar}\langle|\hat{T}|^2\rangle\int_{E_F-eV}^{E_F} D_\sigma(E)D_{\sigma'}(E+eV)dE, \tag{2}$$

where $G_{\sigma,\sigma'}$ represents the tunneling conductance for σ to σ' spin channel. The conductances for the P and AP states are given by $G_P=G_{\uparrow,\uparrow}+G_{\downarrow,\downarrow}$ and $G_{AP}=G_{\uparrow,\downarrow}+G_{\downarrow,\uparrow}$, respectively. In order to calculate Eq. (2), we refer the DOS of $L2_1$-CFAS as shown in Fig. 5(a). The calculated bias voltage dependence of G_P and G_{AP} using Eq. (2) and DOS in Fig. 5(a) are shown in Fig. 5(b) in a positive voltage range (the same for the negative voltage) for $L2_1$-CFAS/MgO/$L2_1$-CFAS structure. The calculated curves can reproduce the experimental result in Fig. 4(a) on the whole; two crossovers between G_P and G_{AP} (corresponding to V_B and V_E) and a local maximum (corresponding to V_D) at around 1.0 V for G_{AP}. The appearance of the maximum around 1.8 eV in G_P in Fig. 5(b) is attributed to the assumed infinite barrier height in the calculation. In fact the effective barrier height of our MgO barrier is determined to be approximately 2 eV by Simmons' fitting for the measured I-V curves.[30] The G_P is almost constant until $V=V_C\sim1.2$ V due to the gap E_g in the minority-spin band of $L2_1$-CFAS [Fig. 5(a)] and no magnon contribution assumed. For further increasing the bias voltage the G_P increases monotonically up to 1.8 V in Fig. 5(b). On the other hand, the G_{AP} is zero until $V=V_A\sim0.5$ V, the conduction-band edge (or the valence-band edge) of the minority-spin band over which the minority-spin electrons start to contribute to the tunneling and G_{AP} increases monotonically in the range of 0.5 V $(V_A)<V<1.1$ V (V_D) with increasing V and gives a inflection point at $V\sim1.1$ V (V_D). The values of the bias voltage V_B and V_E at the first and second crossovers, respectively, are nearly the same as those in Fig. 4(a), respectively, indicating that the plausible band structure of $L2_1$-CFAS calculated. The flat feature within ±0.6 V observed in G_P of $L2_1$-CFAS/MgO/$L2_1$-CFAS [Fig. 4(b)] may support the existence of a wide gap in the vicinity of E_F in the minority band since the total conductance within $|V|<E_g$ must be dominated mainly by majority-majority spin channel for a half-metal/insulator/half-metal MTJ structure.[10] Here, the crossover at a smaller bias voltage in the experiments is not E_g itself but the crossover voltage will be influenced by the existence of the dip, namely, magnon contribution, which changes the shape of the G_{AP} curve. However, the influence is not significant for CFAS with a wide band gap because the magnon contribution is limited to near small bias voltage. The second crossover at V_E mainly reflects the shape of the DOS around -1 eV. In the case of CFAS the DOS of majority-spin band is low and nearly constant down to -1.5 eV, while the DOS of minority-spin band around $-(1-2)$ eV has a deep minimum. This feature provides a maximum around 1.1 V for G_{AP} (V_D). On the other hand, the DOSs of both majority- and minority-spin bands of the CMS increase greatly below -0.5 eV and there is no deep minimum in the minority band.[4,5,8] Consequently, the second crossover and the peak in G_{AP} may not appear in a MTJ using CMS electrodes. In fact, Ishikawa *et al.*[12] reported only one crossover of the conductance curves in a CMS/MgO/CoFe structure.

The only one crossover accompanied with the asymmetric dI/dV curve observed in $L2_1$-CFAS/MgO/$B2$-CFAS structure suggests that the band structure of the $B2$-CFAS differs from that of the $L2_1$-CFAS. The (002) peak intensity in XRD pattern for the $B2$-CFAS annealed at 633 K was weak,[25] suggesting the existing of significant $A2$ or DO_3-type disordering structure in the $B2$-CFAS film, which destroys half metallicity.[21]

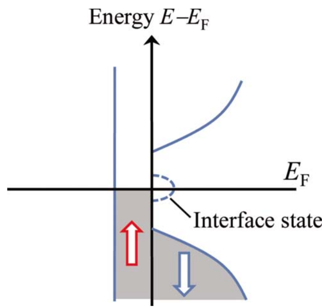

FIG. 6. (Color online) Schematic illustrations of the DOS of the CFAS electrodes.

A crossover in tunneling conductance curves is also reported in the Fe/MgO/Fe structure due to the carbon (C) contamination of the bottom Fe layer.[31] The residual C atoms on a substrate diffuse into bottom Fe/MgO interface and the transport is predicted to be dominated by the Fe-C/MgO electronic structure.[31] In this paper, however, we grew the CFAS/MgO/CFAS structure on a 20-nm-thick MgO buffer layer, which acts as antidiffusion barrier which traps the residual C impurities and prevents their diffusion within the layers during subsequent annealing stages. Therefore, C contamination effect for the crossovers is ruled out in our junctions. In fact, when a 10-nm-thick MgO underlayer was used, the crossover was observed in Fe/MgO/Fe.[31] In addition, we have observed two crossovers accompanied with a peak in the AP curve as seen in Fig. 4(a), which is very different from the C contamination effect.[31]

Recently, we have fabricated MTJs on MgO substrates using an AlO_x barrier consisting of CFAS/AlO_x/CoFe and found 162% TMR ratio at 26 K, which will be reported elsewhere. From this TMR ratio, we obtained $P=0.9$ for CFAS by assuming Julliere's model and $P=0.5$ for CoFe, which implies the half metallicity for CFAS. The smaller $P=0.78$ in the present $L2_1$-CFAS/MgO/$L2_1$-CFAS structure may be attributed to the magnon-assisted inelastic tunneling in a low-bias voltage region.[18] If we assume the interface states near E_F in the minority-spin band gap as shown schematically in Fig. 6, magnon-assisted inelastic tunneling is possible in a low-bias voltage region, which reduces TMR significantly as observed in Fig. 3. The interface states, however, do not affect the spin-dependent tunneling at higher voltages since they lie only near E_F. Thus the two crossovers are maintained even if the interface states assumed near E_F in $L2_1$-CFAS/MgO/$L2_1$-CFAS structure. In the case of the $L2_1$-CFAS/MgO/$B2$-CFAS structure, the top $B2$-CFAS may not be half metallic as mentioned above due to the lower annealing temperature, which leads to the asymmetric conductance without two crossovers as shown in Fig. 4(b).

The other possible reasons of the discrepancy between the experiment and the calculation would be the lower $L2_1$ ordering parameter, which reduces the gap. In fact the gap obtained in this study is about 0.6 eV as seen in Fig. 4(a), while it is 1.2 eV in the calculation. Note that we obtain no distinct proof of the TMR enhancement by the coherent tunneling effect in the present MTJs as mentioned in Sec. III B.

In this study we have used the sputtering method for the MgO barrier formation, which gives a poor-quality barrier as mentioned in Sec. III A. In order to achieve a higher TMR reduction in inelastic tunneling process by realizing clean barrier/CFAS interfaces is required. For this purpose, we would need a high-quality MgO barrier using electron-beam deposition method, which has been performed in the previous experiments of Heusler/MgO/Heusler MTJs.[12–15]

V. CONCLUSIONS

In this work, we measured TMR and tunneling spectroscopy in fully epitaxial MTJs using full-Heusler CFAS/MgO/CFAS structures with $L2_1$ and $B2$ for CFAS layers, fabricated on MgO-buffered MgO (001) substrates using magnetron sputtering. Two distinct crossovers in differential conductance curves G_P and G_{AP} were observed at different voltages for both positive and negative bias voltages in the $L2_1$-CFAS/MgO/$L2_1$-CFAS structure, while only one crossover was observed at a negative voltage in the $L2_1$-CFAS/MgO/$B2$-CFAS structure. We proposed the direct tunneling as a possible transport mechanism leading to the notable crossovers, which reflects the specific spin-dependent density of states of the half-metallic $L2_1$-CFAS. Based on this idea, we calculated G_P and G_{AP} by the DOS for half-metallic $L2_1$-CFAS predicted from first-principle calculations and successfully reproduced the conductance curves as seen in the experiment.

ACKNOWLEDGMENTS

This work was partly supported by the NEDO, the CREST program of the JST, the Grant-in-Aid for Young Scientists (B) under Grant No. 20760478 from the Ministry of Education, Culture, Sports, Science and Technology and JST-SFG project.

*sukegawa.hiroaki@nims.go.jp

[1] R. A. deGroot, F. M. Mueller, P. G. vanEngen, and K. H. J. Buschow, Phys. Rev. Lett. **50**, 2024 (1983).
[2] S. Sugahara and M. Tanaka, Appl. Phys. Lett. **84**, 2307 (2004).
[3] S. Ishida, S. Fujii, S. Kashiwagi, and S. Asano, J. Phys. Soc. Jpn. **64**, 2152 (1995).
[4] I. Galanakis, P. H. Dederichs, and N. Papanikolaou, Phys. Rev. B **66**, 174429 (2002).
[5] S. Picozzi, A. Continenza, and A. J. Freeman, Phys. Rev. B **66**, 094421 (2002).
[6] K. Inomata, S. Okamura, R. Goto, and N. Tezuka, Jpn. J. Appl. Phys., Part 2 **42**, L419 (2003).
[7] J. Schmalhorst, S. Kämmerer, G. Reiss, and A. Hütten, Appl. Phys. Lett. **86**, 052501 (2005).
[8] H. C. Kandpal, G. H. Fecher, C. Felser, and G. Schonhense, Phys. Rev. B **73**, 094422 (2006).

[9] N. Tezuka, N. Ikeda, A. Miyazaki, S. Sugimoto, M. Kikuchi, and K. Inomata, Appl. Phys. Lett. **89**, 112514 (2006).
[10] Y. Sakuraba, T. Miyakoshi, M. Oogane, Y. Ando, A. Sakuma, T. Miyazaki, and H. Kubota, Appl. Phys. Lett. **89**, 052508 (2006).
[11] Y. Sakuraba, M. Hattori, M. Oogane, Y. Ando, H. Kato, A. Sakuma, T. Miyazaki, and H. Kubota, Appl. Phys. Lett. **88**, 192508 (2006).
[12] T. Ishikawa, T. Marukame, H. Kijima, K.-I. Matsuda, T. Uemura, M. Arita, and M. Yamamoto, Appl. Phys. Lett. **89**, 192505 (2006).
[13] T. Marukame, T. Ishikawa, K.-I. Matsuda, T. Uemura, and M. Yamamoto, Appl. Phys. Lett. **88**, 262503 (2006).
[14] N. Tezuka, N. Ikeda, S. Sugimoto, and K. Inomata, Jpn. J. Appl. Phys., Part 2 **46**, L454 (2007).
[15] T. Ishikawa, S. Hakamata, K. Matsuda, T. Uemura, and M. Yamamoto, J. Appl. Phys. **103**, 07A919 (2008).
[16] S. Tsunegi, Y. Sakuraba, M. Oogane, K. Takanashi, and Y. Ando, Appl. Phys. Lett. **93**, 112506 (2008).
[17] M. Julliere, Phys. Lett. **54A**, 225 (1975).
[18] P. Mavropoulos, M. Lezaic, and S. Blugel, Phys. Rev. B **72**, 174428 (2005).
[19] L. Chioncel, Y. Sakuraba, E. Arrigoni, M. I. Katsnelson, M. Oogane, Y. Ando, E. Burzo, T. Miyazaki, and A. I. Lichtenstein, Phys. Rev. Lett. **100**, 086402 (2008).
[20] G. H. Fecher and C. Felser, J. Phys. D **40**, 1582 (2007).
[21] Z. Gercsi and K. Hono, J. Phys.: Condens. Matter **19**, 326216 (2007).
[22] T. M. Nakatani, A. Rajanikanth, Z. Gercsi, Y. K. Takahashi, K. Inomata, and K. Hono, J. Appl. Phys. **102**, 033916 (2007).
[23] S. Yuasa, T. Nagahama, A. Fukushima, Y. Suzuki, and K. Ando, Nature Mater. **3**, 868 (2004).
[24] T. Dimopoulos, G. Gieres, J. Wecker, N. Wiese, Y. Luo, and K. Samwer, J. Appl. Phys. **98**, 073705 (2005).
[25] W. H. Wang, H. Sukegawa, R. Shan, T. Furubayashi, and K. Inomata, Appl. Phys. Lett. **92**, 221912 (2008).
[26] W. H. Wang, H. Sukegawa, R. Shan, and K. Inomata, Appl. Phys. Lett. **93**, 122506 (2008).
[27] X. F. Han, T. Daibou, M. Kamijo, K. Yaoita, H. Kubota, Y. Ando, and T. Miyazaki, Jpn. J. Appl. Phys., Part 2 **39**, L439 (2000).
[28] J. S. Moodera and J. Nowak, R. J. M. vandeVeerdonk, Phys. Rev. Lett. **80**, 2941 (1998).
[29] *Spin Dependent Transport in Magnetic Nanostructures*, edited by S. Maekawa and T. Shinjo (Taylor & Francis, London, 2002).
[30] J. G. Simmons, J. Appl. Phys. **34**, 238 (1963).
[31] C. Tiusan, M. Sicot, J. F.-Vincent, M. Hehn, C. Bellouard, F. Montaigne, S. Andrieu, and A. Schuhl, J. Phys.: Condens. Matter **18**, 941 (2006).